Highly Sensitive Refractive Index Sensor based on Photonic Crystal Ring Resonators Nested in a Mach-Zehnder Interferometer

Amir Hossein Abdollahi Nohoji
Semnan University
Mohammad Danaie (Danaie@semnan.ac.ir)
Semnan University https://orcid.org/0000-0001-7046-2794

Research Article

Keywords: Micro-ring resonator, Mach-Zehnder interferometer, Refractive index sensor, Sensitivity, Finite difference time domain (FDTD)

Posted Date: March 3rd, 2022

DOI: https://doi.org/10.21203/rs.3.rs-1396678/v1

Abstract

Today, with the rapid development of photonics, optical sensors are being considered as efficient tools for detecting environmental variations and have been regarded as one of the most important fields in photonic research. In this study, we have proposed a two-dimensional photonic crystal (2D-PC) refractive index sensor using a combination of Mach-Zehnder interferometers and two ring resonators. Our goal is to increase the sensitivity and figure of merit (FOM) of the sensor, so that the output transmission spectrum can be considerably shifted by changing the refractive index of the simulated analytes. The proposed photonic crystal sensor consists of a hexagonal array of silicon rods on a SiO_2 substrate. The finite difference time domain (FDTD) method is used for the numerical simulation of the structure. In this regard, to validate the simulation results, two different commercial software have been used. The quality-factor (Q-factor) and the sensitivity of the proposed structure are more than 1600 and 1700 nm / RIU, respectively, where RIU stands for the refractive index unit. In general, the structure has advantages such as low fabrication cost, high sensitivity to changes in refractive index and a high Q-factor.

1. Introduction

Today rapid growth of photonic nanotechnology sciences has led to development of devices such as sensors, modulators, optical fibres, switches, etc. Refractive index (RI) sensors are used in a wide variety of physical detectors to measure the concentration of liquids and gases [1–2]. Mach Zehnder's interferometer (MZI) [3–4] and micro-loop amplifiers (MRR) [5–7] are not only widely used in optical circuits, but have also recently been used as optical biosensors. So far, various optical sensors have been proposed to detect refractive index changes designed from different structures, such as Mach Zander interferometers [8–13], Ring Resonators [14–17], Fabry-Perot interferometers (FPI) [18]. A Mach-Zander interferometer can be simulated using FDTD while it consists of an optical y-splitter and a y- combiner waveguide. In [19] the bending radius of Y waveguides at 385 μm and the average free spectral range (FSRs) of 18 nm are optimized for the MZI model. Also, a MZI can be used as an optical switch. A low-consumption MZI have been presented as a photonic crystal switch using a phase change material (PCM) [20]. Also, MRRs can be used in the nonlinear mode as an all-optical switch or sensor to shift the resonant wavelength by changing the refractive index [21].

In this study, we demonstrated the combination of MRR with MZI as a highly sensitive RI sensor. For the presented topology, the transmission spectrum experiences a considerable wavelength shift as a result of analyte's RI change. In fact, we used two MRRs nested in an MZI and showed that a small change in refractive index could cause a large change in the resonance wavelength of the structure.

2. Structure Design

In this structure, an optical splitter and a combiner connected to two straight waveguides are used to design a photonic crystal MZI. The structure is designed using a hexagonal array of silicon rods in an air background. The optical response of the structure is obtained using the Lumerical's FDTD Solver. Two

photonic crystal rings resonators (PhCRR) are located between straights waveguide arms. Typically, each ring resonator is formed by removing rods in the original photonic crystal (PhC) lattice. The structure is shown in Fig. 1. The lattice constant and the diameter of the rods are considered to be 1μm and 200 nm, respectively. To determine the refractive index of the analyte, the structure can be placed in the analyte. The refractive index of silicon and water as analytes are approximately 3.436 and 1.33 at the wavelength range of 2900 to 3100 nm, respectively.

In fact, each of the PhCRR arms acts separately in both through and drop ports [22–23]. Figure 2 shows a PhCRR designed in the PhC lattice. Using the splitter, half of the source wave is divided in each of the straight waveguide arms. Each arm plays the role of through and drop relative to each other (Fig. 2). In the photonic crystal ring resonator nested in Mach-Zehnder interferometer (RR-MZI), light is evenly distributed on both splitter arms and then coupled to the PhCRRs from each side up and down. Actually, at the resonant wavelength, both PCRRs act as one meta-ring resonator.

3. Simulation And Optimization

The photonic band structure in the normalized frequency range of 0.28 to 0.37 [a/λ] for the transverse magnetic state (TM) is shown in Fig. 3. In fact, wavelengths between 2700 and 3500 nm can pass through the structure's waveguides.

At the input wavelength of 2971 nm, when the whole structure is immersed in water as an analyte, both RRs are paired. Consequently, light passes through MZI arms and it is later collected in the combinator and transmitted to the output port of MZI. At this wavelength, the maximum amount of light reaches the output port, where the normalized transmission is equal to 0.82. By a 13 nm shift in the input wavelength, the structure will not allow light to pass through, resulting in the MZI output being minimized (Fig. 4a). This results a quality factor (Q-factor) [24–28] approximately equal to 1500. Eq. (1) shows the relationship used for calculation of the Q-factor of the photonic crystal ring resonators.

$$Q\_factor = \frac{\lambda(peakresonance)}{FWHMBandwidth} \quad (1)$$

Where, FWHM is the full width at half maximum (measured using the transmission spectrum). For validation, the results obtained using two different commercial software (Rsoft photonics CAD suite and Ansys Lumerical) have been superimposed in Fig. 4(b), which shows a very good similarity.

To optimize the structure, four rods (a and b) have been added at the MZI input and output (Fig. 5). The optimum radii of rods a and b were obtained by sweeping as 185 and 100 nm, respectively. The normalized transmission of the optimized structure increased from 0.82 to 0.93 (Fig. 6). Also, the Q-factor increase from 1518 to 1560.

The sensitivity [29–34] of the structure is also calculated as follows:

$$S = \frac{\Delta\lambda\,(peak)}{\Delta n_{analyte}} \left[\frac{nm}{RIU}\right] \quad (2)$$

Where, $\Delta\lambda$ is the change in resonance peak while the refractive index of analyte changes with the value of Δn. The sensitivity of the structure is about 1640 [nm/RIU], which indicates a good separation. Figure 7 shows the normalized transmission for different refractive indices.

The figure of merit [35–37] (FoM) is a parameter for comparing the performance of sensors, which is defined as follows:

$$FOM = \frac{\frac{\Delta\lambda}{\Delta n}}{FWHM} = \frac{S}{FWHM} \quad (3)$$

The resonance wavelength and Q-factor for different analyte refractive indices are plotted in Fig. 8(a), Fig. 8(b), respectively. Also, the sensitivity and FOM of the sensor are shown in Fig .8(c), Fig. 8(d), respectively. Actually, with increasing the refractive index of the analyte, the Q-factor increases and the sensitivity and FOM decreases. The FWHM bandwidth for the refractive indexes of the various analytes is about 1.95 nm, and the average FOM of sensor is about 840 RIU^{-1}.

4. Discussion And Comparisons

In this section, the performance of different RI sensors is compared with the proposed structure. The electric field for the optimized structure (shown in the Fig. 5) shows that at the input wavelength of 2959 nm, both PCRRs are coupled together and light passes through the straight waveguides and it is transmitted to the MZI output port. Instead, at 2946 nm, no signal is directed to MZI output. The electric field intensities though the structure are shown in Fig. 9(a) and Fig. 9(b).

Some of the best refractive index sensors are listed in Table 1, where the resolution of the sensors is determined by the following equation:

$$R = \frac{\Delta n_{analyte} \times \Delta\lambda_{min}}{\Delta\lambda_{(peak)}}(RIU) \quad (4)$$

Table 1
Performance comparison of Refractive Index Sensitive Sensor based on Photonic Crystal

Structure	RI Range (RIU)	Sensitivity (nm/RIU)	Resolution (RIU)	Q-factor	Figure of merit (RIU − 1)	Ref.
ring cavity	1.33–1.44	536–600	1.24×10 − 4	1432–2081	487	[37]
PCF with up-tapered joints	1.333–1.379	252	8 × 10 − 5			[38]
PCF-MZI with two HTCRS	1.3333–1.3574	181.96				[39]
Cladding Etched PFC MZI	1.333–1.381	359.37	4.73 × 10−5			[40]
H-shaped PCF coated with silver and graphene	1.33–1.36	2770	3.61*10 − 6			[41]
T-shaped PC	1.05–1.10	1040				[42]
ring-shaped slotted PC	1–1.5	1450				[43]
MIM-plasmonic ring shaped	1- 1.2	636		269	211.3	[44]
Fano resonance	1_1.4	1060		145	176.7	[45]
Current work	1.33_1.37	1640	6*10 − 5	1535	840	

5. Conclusions

We have proposed a sensitive refractive index sensor based on photonic crystal ring resonators nested in a Mach-Zehnder interferometer. The sensor structure is simulated using FDTD method and has a good quasi-linear sensitivity to changes in the refractive index of the analyte. In the RI range of 1.33 to 1.37 the average values of Q-factor and sensitivity are 1535 and 1640 (nm/RIU), respectively. Also, the average FOM in this work was calculated about 840 RIU^{-1}. Finally, the proposed structure is a good candidate for sensor design, to determine the refractive index or to identify different analytes.

Declarations

Author Contribution

Design, analysis, and investigation: Amir Hossein Abdollahi Nohoji, Writing—original draft preparation: Amir Hossein Abdollahi Nohoji, Writing—review and editing: Mohammad Danaie, Supervision: Mohammad Danaie. **Availability of Data and Materials** The datasets generated and analyzed during the current study are available from the corresponding author on reasonable request.

Ethical Approval We the undersigned declare that the manuscript entitled “Highly Sensitive Refractive Index Sensor based on Photonic Crystal Ring Resonators Nested in a Mach-Zehnder Interferometer” is original, has not been fully or partly published before, and is not currently being considered for publication elsewhere. Also, results are presented clearly, honestly, and without fabrication, falsification, or inappropriate data manipulation. We confirm that the manuscript has been read and approved by all named authors and that there are no other persons who satisfied the criteria for authorship but are not listed. We further confirm that the order of authors listed in the manuscript has been approved by all of us.

Conflict of Interest The authors declare no conflict of interests.

References

1. Wo, J.H., Wang, G.H., Cui, Y., Sun, Q., Liang, R.B., Shum, P., et al.: Refractive index sensor using microfiber-based Mach-Zehnder interferometer. Opt. Lett. **37**(1), 67–69 (2012) “,”,)
2. Sun, X.Y., Dong, X.R., Hu, Y.W., Li, H.T., Chu, D.K., Zhou, J.Y., et al.: A robust high refractive index sensitivity fiber Mach-Zehnder interferometer fabricated by femtosecond laser machining and chemical etching. Sens. Actuators A: Phys. **230**, 111–116 (2015) “,”,
3. Zhao, Y., Xia, F., Hu, H.F., Chen, M.Q.: A novel photonic crystal fiber Mach–Zehnder interferometer for enhancing refractive index measurement sensitivity. Opt. Commun. **1**, 402:368–374 (2017 Nov)
4. Du, H., Sun, X., Hu, Y., Dong, X., Zhou, J.: High sensitive refractive index sensor based on cladding etched photonic crystal fiber Mach-Zehnder interferometer. Photonic Sens. **9**(2), 126–134 (2019 Jun)
5. Rahmatiyar, M., Afsahi, M., Danaie, M.: Design of a refractive index plasmonic sensor based on a ring resonator coupled to a MIM waveguide containing tapered defects. Plasmonics **15**(6), 2169–2176 (2020 Dec)
6. Sumetsky, M., Windeler, R.S., Dulashko, Y., Fan, X.: Optical liquid ring resonator sensor. Optics Express. 2007 Oct 29;15(22):14376–81
7. Wang, Q., Hamadeh, A., Verba, R., Lomakin, V., Mohseni, M., Hillebrands, B., Chumak, A.V., Pirro, P.: A nonlinear magnonic nano-ring resonator. npj Computational Materials. 2020 Dec 14;6(1):1–7
8. Lu, P., Men, L.Q., Sooley, K., Chen, Q.: Tapered fiber Mach-Zehnder interferometer for simultaneous measurement of refractive index and temperature. Appl. Phys. Lett. **94**(13), 131110-1–131110-3 (2009) “,”,)
9. Sun, X.Y., Chu, D.K., Dong, X.R., Zhou, C., Li, H.T., Zhi, L., et al.: Highly sensitive refractive index fiber inline Mach-Zehnder interferometer fabricated by femtosecond laser micromachining and chemical etching. Opt. Laser Technol. **77**, 11–15 (2016) “,”,
10. Du, H., Sun, X., Hu, Y., Dong, X., Zhou, J.: High sensitive refractive index sensor based on cladding etched photonic crystal fiber Mach-Zehnder interferometer. Photonic Sens. **9**(2), 126–134 (2019 Jun)
11. Pawar, D., Kale, S.N.: Birefringence manipulation in tapered polarization-maintaining photonic crystal fiber Mach-Zehnder interferometer for refractive index sensing. Sens. Actuators A: Phys. **252**, 180–

184 (2016) “,”,

12. Wu, D., Zhao, Y., Li, J.: PCF taper-based Mach-Zehnder interferometer for refractive index sensing in a PDMS detection cell. Sens. Actuators B: Chem. **213**, 1–4 (2015) “,”,
13. Zhao, Y., Xia, F., Hu, H.F., Chen, M.Q.: A novel photonic crystal fiber Mach-Zehnder interferometer for enhancing refractive index measurement sensitivity. Opt. Commun. **402**, 368–374 (2017) “,”,
14. Arunkumar, R., Suganya, T., Robinson, S.: Design and analysis of photonic crystal elliptical ring resonator based pressure sensor. Int. J. Photonics Opt. Technol. **1**(3), 30–33 (2017 Mar)
15. Jannesari, R., Ranacher, C., Consani, C., Lavchiev, V., Grille, T., Jakoby, B.: High-Quality-Factor Photonic Crystal Ring Resonator with Applications for Gas Sensing. Procedia Eng. **1**, 168:375–379 (2016 Jan)
16. Radhouene, M., Chhipa, M.K., Najjar, M., Robinson, S., Suthar, B.: Novel design of ring resonator based temperature sensor using photonics technology. photonic Sens. **7**(4), 311–316 (2017 Dec)
17. Hsiao, F.L., Lee, C.: Novel biosensor based on photonic crystal nano-ring resonator. Procedia Chem. **1(1)**(1), 417–420 (2009 Sep)
18. Wei, T., Han, Y.K., Li, Y.J., Tsai, H.L., Xiao, H.: Temperature-insensitive miniaturized fiber inline Fabry-Perot interferometer for highly sensitive refractive index measurement. Opt. Express **16**(8), 5764–5769 (2008) “,”,)
19. Tasaki, K., et al.: "Nested Mach–Zehnder interferometer optical switch with phase generating couplers." Japanese Journal of Applied Physics 59.SO (2020)
20. Kumar, K., Vinay, et al.: "Photonic Crystal Mach-Zehnder Optical Switch Based on Phase Change Material." 2020 IEEE 20th International Conference on Nanotechnology (IEEE-NANO). IEEE, 2020
21. Rakshita Rakshit, J., Chattopadhyay, T., Roy, J.: Design of ring resonator based all optical switch for logic and arithmetic operations - A theoretical study. Optik. **124**, 6048–6057 (2013)
22. Sreenivasulu, T., Bhowmick, K., Samad, S.A., Yadunath, T.I., Badrinarayana, T., Hegde, G.M., Srinivas, T.: Photonic crystal ring resonator-based four-channel dense wavelength division multiplexing demultiplexer on silicon on insulator platform: design and analysis. Opt. Eng. **57**(4), 046109 (2018 Apr)
23. Robinson, S., Nakkeeran, R.: Photonic crystal ring resonator-based add drop filters: a review. Opt. Eng. **52**(6), 060901 (2013 Jun)
24. Siraji, A.A., Zhao, Y.: High-sensitivity and high-Q-factor glass photonic crystal cavity and its applications as sensors. Optics letters. 2015 Apr 1;40(7):1508-11
25. Saha, P., Sen, M.: A slotted photonic crystal nanobeam cavity for simultaneous attainment of ultra-high Q-factor and sensitivity. IEEE Sensors Journal. 2018 Mar 8;18(9):3602–9
26. Kolli, V.R., Bahaddur, I., Prabhakar, D., Talabattulac, S.: A high Q-factor photonic crystal microring-resonator based pressure sensor. Photonics and Nanostructures-Fundamentals and Applications. 2021 Feb 1;43:100870

27. Rebhi, S., Najjar, M.: High Q-factor optical filter with high refractive index sensitivity based on hourglass-shaped photonic crystal ring resonator. Optik. 2020 Feb 1;202:163663
28. Olyaee, S., Mohebzadeh-Bahabady, A.: Two-curve-shaped biosensor using photonic crystal nano-ring resonators. Journal of Nanostructures. 2014 Jul 1;4(3):303-8
29. Zhao, Y., Xia, F., Li, J.: Sensitivity-enhanced photonic crystal fiber refractive index sensor with two waist-broadened tapers. Journal of Lightwave Technology. 2016 Feb 15;34(4):1373–9
30. Rindorf, L., Bang, O.: Sensitivity of photonic crystal fiber grating sensors: biosensing, refractive index, strain, and temperature sensing. JOSA B. 2008 Mar 1;25(3):310 – 24
31. Aly, A.H., Zaky, Z.A.: Ultra-sensitive photonic crystal cancer cells sensor with a high-quality factor. Cryogenics **1**, 104:102991 (2019 Dec)
32. Olyaee, S., Mohebzadeh-Bahabady, A.: Two-curve-shaped biosensor using photonic crystal nano-ring resonators. Journal of Nanostructures. 2014 Jul 1;4(3):303-8
33. Liu, C., Su, W., Liu, Q., Lu, X., Wang, F., Sun, T., Chu, P.K.: Symmetrical dual D-shape photonic crystal fibers for surface plasmon resonance sensing. Optics express. 2018 Apr 2;26(7):9039-49
34. Liang, H., Shen, T., Feng, Y., Liu, H., Han, W.: A D-Shaped photonic crystal fiber refractive index sensor coated with graphene and zinc oxide. Sensors. **21**(1), 71 (2021 Jan)
35. Alfimov, M.V., Zheltikov, A.M.: The figure of merit of a photonic-crystal fiber beam delivery and response-signal collection for nanoparticle-assisted sensor arrays. Laser Physics Letters. 2006 Dec 21;4(5):363
36. Chowdhury, S., Maity, A.: Numerical analysis of photonic crystal fiber based hemoglobin sensor. Optik **1**, 130:825–829 (2017 Feb)
37. Rahman-Zadeh, F., Danaie, M., Kaatuzian, H.: Design of a highly sensitive photonic crystal refractive index sensor incorporating ring-shaped GaAs cavity. Opto-Electronics Review. 2019 Dec 1;27(4):369 – 77
38. Zhao, Y., Li, X.G., Cai, L., Yang, Y.: Refractive index sensing based on photonic crystal fiber interferometer structure with up-tapered joints. Sensors and Actuators B: Chemical. 2015 Dec 31;221:406–10
39. Zhao, Y., Xia, F., Hu, H.F., Chen, M.Q.: A novel photonic crystal fiber Mach–Zehnder interferometer for enhancing refractive index measurement sensitivity. Opt. Commun. **1**, 402:368–374 (2017 Nov)
40. Du, H., Sun, X., Hu, Y., Dong, X., Zhou, J.: High sensitive refractive index sensor based on cladding etched photonic crystal fiber Mach-Zehnder interferometer. Photonic Sens. **9**(2), 126–134 (2019 Jun)
41. Li, T., Zhu, L., Yang, X., Lou, X., Yu, L.: A refractive index sensor based on H-shaped photonic crystal fibers coated with Ag-graphene layers. Sensors **20**(3), 741 (2020 Jan)
42. Turduev, M., Giden, I.H., Babayiğit, C., Hayran, Z., Bor, E., Boztuğ, Ç, Kurt, H., Staliunas, K.: Mid-infrared T-shaped photonic crystal waveguide for optical refractive index sensing. Sens. Actuators B **1**, 245:765–773 (2017 Jun)

43. Kassa-Baghdouche, L., Cassan, E.: Sensitivity analysis of ring-shaped slotted photonic crystal waveguides for mid-infrared refractive index sensing. Opt. Quant. Electron. **51**(10), 1–1 (2019 Oct)
44. Danaie, M., Shahzadi, A.: Design of a high-resolution metal–insulator–metal plasmonic refractive index sensor based on a ring-shaped Si resonator. Plasmonics. **14**(6), 1453–1465 (2019 Dec)
45. Zafar, R., Salim, M.: Enhanced figure of merit in Fano resonance-based plasmonic refractive index sensor. IEEE Sensors Journal. 2015 Jul 17;15(11):6313–7

Figures

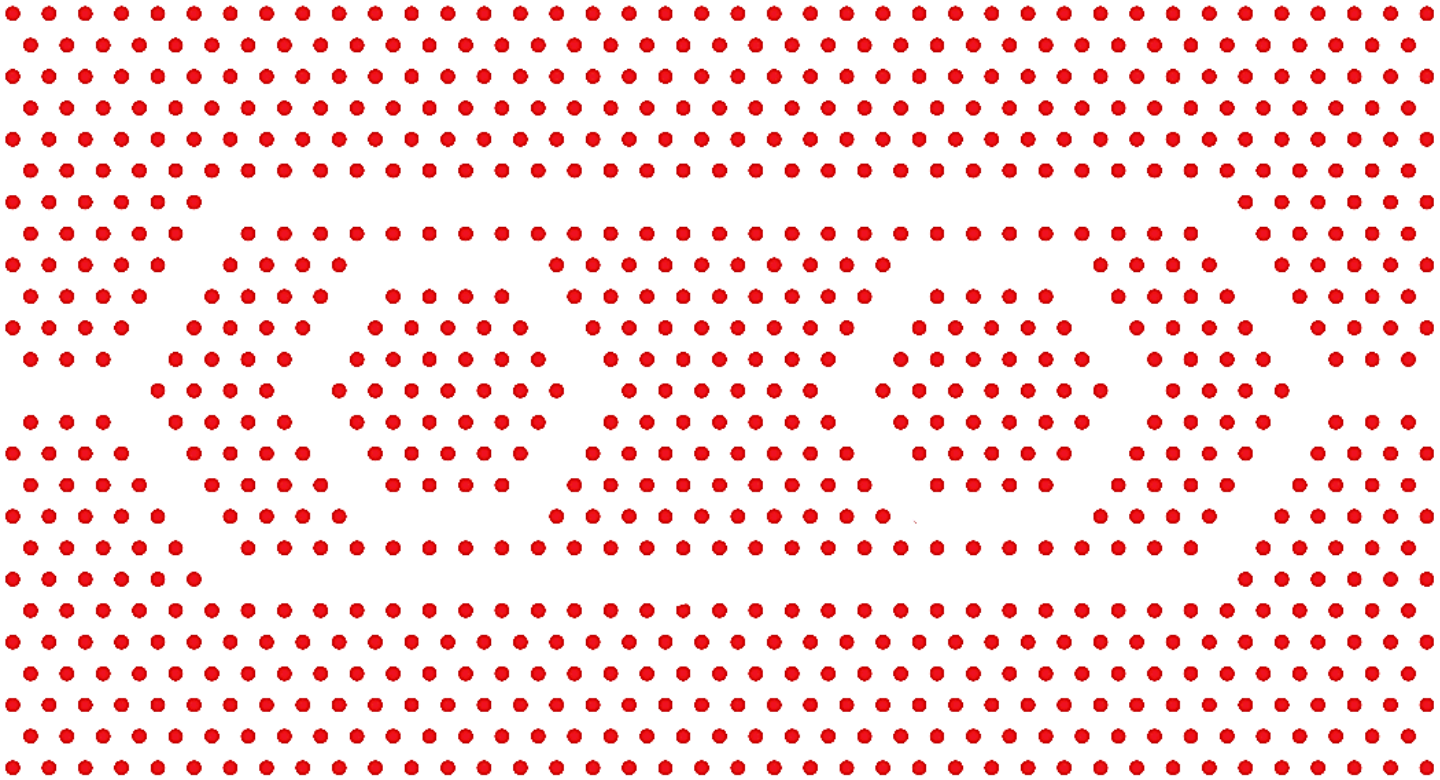

Figure 1

The photonic crystal RRs nested in a PhC MZI structure.

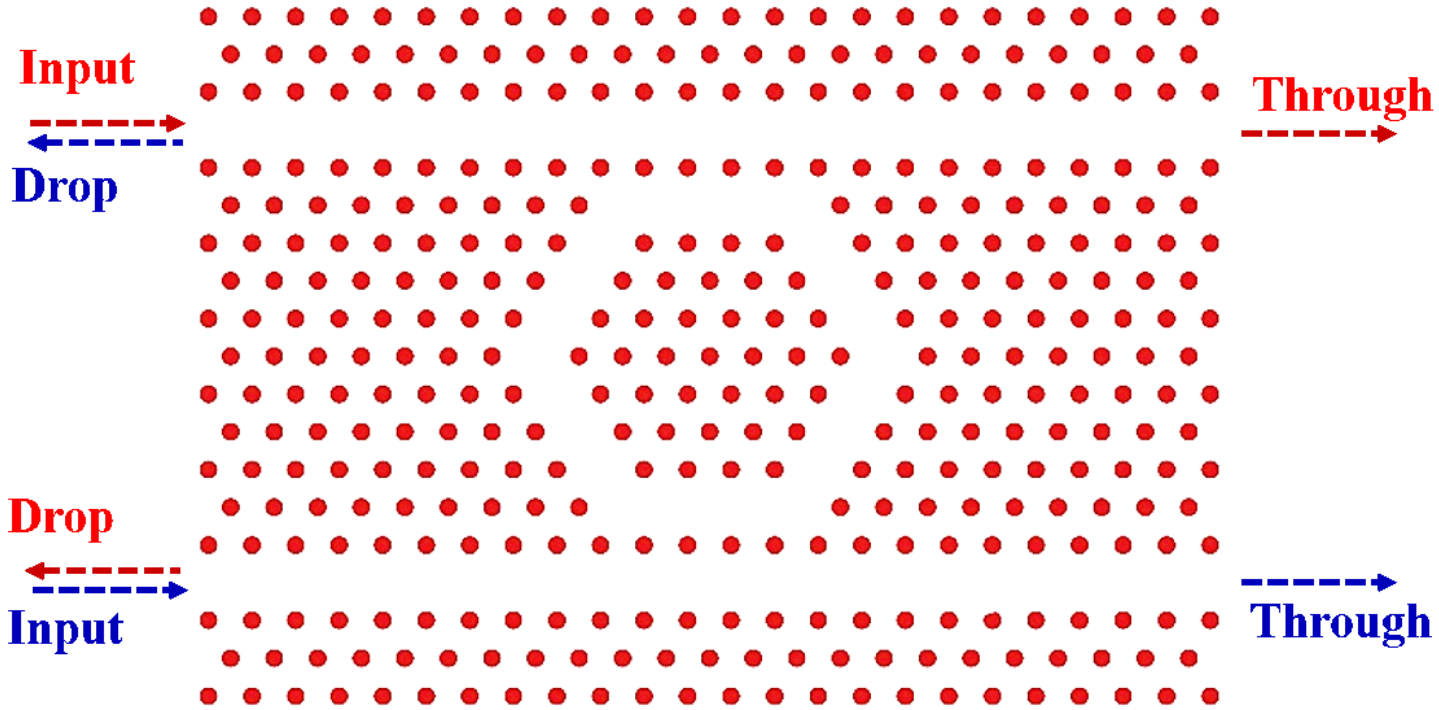

Figure 2

A photonic crystal ring resonator.

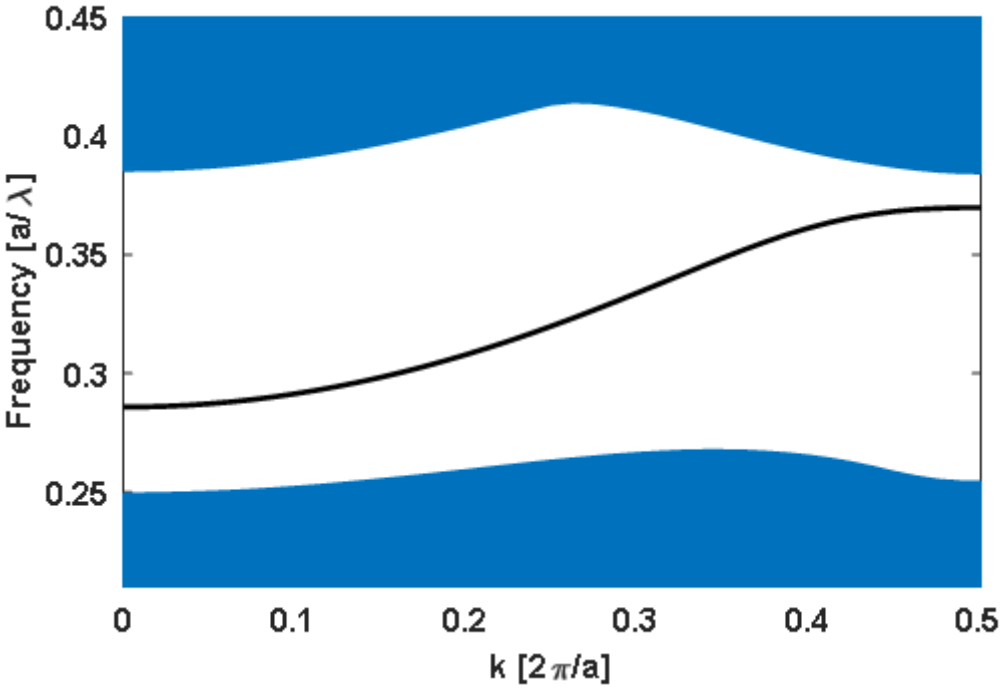

Figure 3

The band structure of optimized proposed sensor.

Figure 4

(a) Output normalized transmission at 2971 nm with water as analyte, (b) The normalized transmission comparison using Rsoft and Lumerical simulators using the FDTD method.

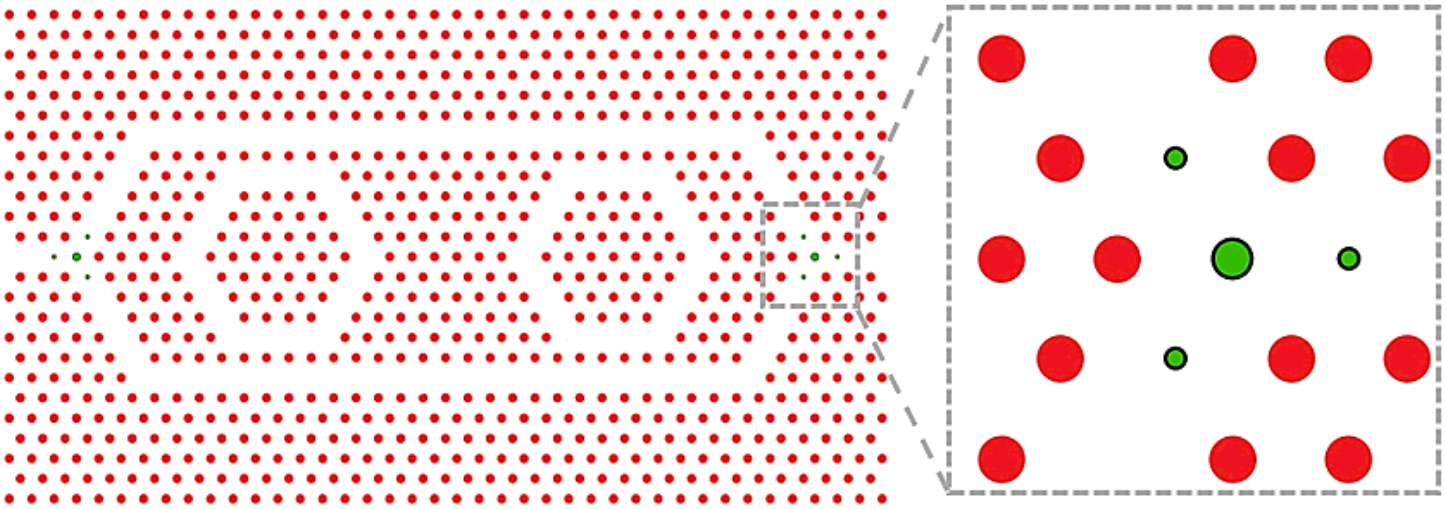

Figure 5

The optimized structure

Figure 6

The transmission spectrum for the optimized structure presented in Fig. 5.

Figure 7

The transmission spectrum for refractive indices of different analytes.

Figure 8

The resonance wavelength versus analyte's refractive index, (b), Q-factor versus analyte's refractive index, (c) Sensitivity versus analyte's refractive index, (d) The FOM of the sensor versus analyte's refractive index.

Figure 9

The electric field intensity for the optimized structure, (a) at the wavelength of 2959 nm (b) at the wavelength of 2946 nm.